Increasing Earth System Sensitivity in mid-Pliocene simulations from CCSM4 to CESM2

Ran Feng[1], Otto-Bliesner Bette L.[2], Esther C. Brady[3], and Nan A. Rosenbloom[3]

[1]University of Connecticut
[2]Climate and Global Dynamics Division, National Center for Atmospheric Research (NCAR), Boulder, CO 80305, USA
[3]National Center for Atmospheric Research (UCAR)

November 24, 2022

Abstract

Three new equilibrium Mid-Pliocene (MP) simulations are implemented with the Community Climate System Model version 4 (CCSM4), Community Earth System Model version 1.2 (CESM1.2), and 2 (CESM2). All simulations are carried out with the same boundary and forcing conditions following the protocol of Pliocene Model Intercomparison Project Phase 2. These simulations reveal amplified MP climate change relative to preindustrial going from CCSM4 to CESM2, seen in global mean and polar amplification of surface warming, sea ice reduction in both Arctic and Antarctic, and weakened Hadley circulation. The enhanced global mean warming arises from both enhanced Earth System Sensitivity (ESS) and Equilibrium Climate Sensitivity (ECS) to CO forcing. ESS is amplified by up to 70% in CCSM4, and up to 100% in CESM1.2 and CESM2 relative to ECSs of respective models. Simulations also agree on the strengthened Atlantic Meridional Overturning Circulation, but disagree on several other climate metrics. Compared to preindustrial, CCSM4 features small increase in both low and high cloud cover and no change in the mean climate state of the equatorial Pacific. Whereas, both CESM1.2 and 2 show reduction of cloud cover at all heights, and an anomalous El Niño-like state of the equatorial Pacific. The performances of MP simulations are assessed with a new compilation of paleo-observations of sea surface temperature (SST). CESM1.2 and 2 show better skills than CCSM4 in simulating MP global mean warming and amplified SST warming in the northern middle and high latitudes, supporting the amplified ESS compared to the CCSM4.

Increasing Earth System Sensitivity in mid-Pliocene simulations from CCSM4 to CESM2

Ran Feng[1], Bette Otto-Bliesner[2], Esther Brady[2], and Nan Rosenbloom[2]

[1]Department of Geosciences, University of Connecticut

[2]National Center for Atmospheric Research

Corresponding author: Ran Feng (ran.feng@uconn.edu)

Key Points:

- PlioMIP2 simulations are completed with three versions of Earth System Models from the NCAR family
- Simulated mid-Pliocene climate features greater changes in many climate metrics relative to preindustrial in the newer models
- The newer models show greater Earth System Sensitivity and match paleo-observations better than the old model

Abstract

Three new equilibrium Mid-Pliocene (MP) simulations are implemented with the Community Climate System Model version 4 (CCSM4), Community Earth System Model version 1.2 (CESM1.2), and 2 (CESM2). All simulations are carried out with the same boundary and forcing conditions following the protocol of Pliocene Model Intercomparison Project Phase 2. These simulations reveal amplified MP climate change relative to preindustrial going from CCSM4 to CESM2, seen in global mean and polar amplification of surface warming, sea ice reduction in both Arctic and Antarctic, and weakened Hadley circulation. The enhanced global mean warming arises from both enhanced Earth System Sensitivity (ESS) and Equilibrium Climate Sensitivity (ECS) to CO_2 forcing. ESS is amplified by up to 70% in CCSM4, and up to 100% in CESM1.2 and CESM2 relative to ECSs of respective models. Simulations also agree on the strengthened Atlantic Meridional Overturning Circulation, but disagree on several other climate metrics. Compared to preindustrial, CCSM4 features small increase in both low and high cloud cover and no change in the mean climate state of the equatorial Pacific. Whereas, both CESM1.2 and 2 show reduction of cloud cover at all heights, and an anomalous El Niño-like state of the equatorial Pacific. The performances of MP simulations are assessed with a new compilation of paleo-observations of sea surface temperature (SST). CESM1.2 and 2 show better skills than CCSM4 in simulating MP global mean warming and amplified SST warming in the northern middle and high latitudes, supporting the amplified ESS compared to the CCSM4.

Plain Language Summary

Our knowledge of past climate evolves with both new paleo-observations and new advancements in modeling past climates. Using mid-Pliocene (3.205 Millions of years ago) as an example, we demonstrate how to implement geological reconstructions of past topography, bathymetry, and vegetation distribution in Earth System Model (ESM) simulations, how to initialize these experiments, and finally, the new knowledge learnt from the newer versions of the ESMs. In our simulations with a 400 ppm CO_2, when millennial time-scale changes of biome range, ocean circulation, and ice sheet are considered, the mid-Pliocene Earth system warms substantially more than the estimates that do not consider these changes. The simulated mid-Pliocene climate features strongly amplified polar warmth, massive loss of Arctic and Antarctic summer sea ice, and weakened northern hemispheric cell of the Hadley circulation. More intriguingly, the newer ESMs are more sensitive to CO_2 and prescribed millennial time-scale changes in boundary conditions than the old model, yet they match paleo-observations much better. This result suggests that the newer models are more in line with paleo-observations, and that the climate change at millennial time-scale is underestimated by the old model.

1 Introduction

Mid-Piacenzian (or Mid-Pliocene) Warm period (MP for short, at 3.205 Millions of years ago, Ma) has been identified as one of the key targets of Paleoclimate Model Intercomparison Project (PMIP) (Haywood, Dolan, Pickering, Dowsett, McClymont, Prescott, Salzmann, Hill, Hunter, & Lunt, 2013a; Masson-Delmotte et al., 2013). Despite good agreement in simulating modern and pre-industrial climate, Earth System models (ESMs) diverge in predicting many fundamental aspects of future climate change, including the transient melting behavior of the Arctic Sea ice (Stroeve et al., 2012), Arctic feedbacks (Pithan & Mauritsen, 2014), changes in equatorial Pacific SST pattern (Coats & Karnauskas, 2017; Seager et al., 2019), changes in subtropical precipitation (Collins et al., 2013), among many others. Paleo-observations can provide independent out-of-sample data to help constrain these uncertainties (Haywood, Valdes, Aze, Barlow, Burke, Dolan, Heydt, Hill, Jamieson, & Otto-Bliesner, 2019a; Kageyama et al., 2018). To this end, Pliocene Model Intercomparison Project (PlioMIP) (Haywood, Dowsett, & Dolan, 2015; Haywood et al., 2010) and Pliocene Research, Interpretation and Synoptic Mapping Project (PRISM) (Dowsett et al., 2013; 2010) were carried out with separate focuses on paleoclimate modeling and paleo-observational data synthesis. The simulations featured in the current study contribute to the second phase of PlioMIP (PlioMIP2).

PlioMIP2 targets at the time slice of 3.205 Ma during the Mid-Piacenzian, MP for short (Dowsett et al., 2013; Haywood, Dolan, Pickering, Dowsett, McClymont, Prescott, Salzmann, Hill, Hunter, Lunt, et al., 2013b). The selection of 3.205 Ma allows the alignment of model simulations with interglacial of marine isotope stage (MIS) KM5C (Prescott, Haywood, Dolan, & Hunter, 2014), which occurred with present-day orbits and 400 ppm CO_2 (Haywood, Dolan, Pickering, Dowsett, McClymont, Prescott, Salzmann, Hill, Hunter, Lunt, et al., 2013b). The Greenland ice sheet is prescribed with results from the Pliocene Ice Sheet Modeling Project (Dolan, Koenig, Hill, Haywood, & DeConto, 2012). This new ice sheet configuration features substantial reduction in ice coverage with only 25% modern coverage located in the Eastern

Greenland Mountains and deglaciated western Antarctic (Dowsett, Dolan, Rowley, Moucha, Forte, Mitrovica, Pound, Salzmann, Robinson, & Chandler, 2016a). Global soil map is generated for MP (Pound, Tindall, Pickering, Haywood, et al., 2014b). A dynamic topography model is applied to estimate topographic changes due to changes in mantle convection and removal of ice sheets (Dowsett, Dolan, Rowley, Moucha, Forte, Mitrovica, Pound, Salzmann, Robinson, & Chandler, 2016b). Sea level and sedimentary information are integrated with simulations of dynamic topography to determine changes to the ocean gateways and costal shelf, resulting in closed Bering strait, closed Canadian Archipelago straits, exposed Sunda and Sahul Shelf in marine time continents, and exposed Baltic shelf and Hudson bay (Dowsett, Dolan, Rowley, Moucha, Forte, Mitrovica, Pound, Salzmann, Robinson, & Chandler, 2016a).

In the modeling realm, following the previous PlioMIP (PlioMIP1), many new versions of Earth System Models (ESMs) are released, including Community Earth System Model version 1 and 2 (CESM1 and 2). PlioMIP1 has been carried out with the Community Climate System Model version 4 (CCSM4) (Rosenbloom, Otto-Bliesner, Brady, & Lawrence, 2013a). Different from CCSM4, CESM1 features extensive updates in representing atmospheric physics including new radiation calculation, boundary layer scheme, shallow convection scheme, and cloud microphysics (Hurrell et al., 2013). The model also incorporates a modular aerosol model (Liu et al., 2012). CESM1 shows improved simulations of cloud climatology and radiative forcing compare to CCSM4 (Kay et al., 2012), and substantial changes in cloud feedback to CO_2 warming with overall less cloud cooling effect in response to surface warming (Gettelman, Kay, & Shell, 2012). CESM1 also has a higher equilibrium climate sensitivity (ECS) of 4 K per doubling of CO_2 (Gettelman, Kay, & Fasullo, 2013). ECS is 3.2 K in CCSM4 (Bitz et al., 2012). In published CESM1.2 PlioMIP1 simulations, the capability of simulating aerosol cloud interactions and the removal of anthropogenic pollutants are shown to substantially amplify the Arctic warmth (Feng et al., 2019). The combined changes of atmospheric physics in CESM1.2 also produce an anomalous El Niño-like equatorial Pacific response in CESM1.2 PlioMIP1, which is not featured in CCSM4 PlioMIP1 (Tierney, Haywood, Feng, Bhattacharya, & Otto-Bliesner, 2019).

From CESM1 to CESM2, substantial updates are made to all model components (Danabasoglu, Lamarque, & Bachmeister, et al., 2019). In particular, the new land model features substantial changes in both CO_2 and nitrogen fertilization (Fisher et al., 2019). Parameterizations of planetary boundary layer and shallow convection are now unified with the Cloud Layers Unified by Bi-Normals Parameterization (CLUBB) (Bogenschutz et al., 2013). Sea ice model has now included the mushy layer physics (Turner & Hunke, 2015). ECS has increased again to 5 K per doubling of CO_2 (Gettelman et al., 2019).

In this study, we document the implementation of this new set of MP boundary conditions in three generations of models from the same lineage: CCSM4, CESM1.2, and CESM2, and quantify simulated large-scale MP climate changes relative to preindustrial (PI). Model convergence and divergence are highlighted. A new compilation of paleo-observations of sea surface temperature (SST) (Foley & Dowsett, 2019) are used to evaluate performances of different MP simulations.

2 Materials and Methods

2. 1 Experiments

2.1.1 Model components, resolution, and new ocean grid mesh created for PlioMIP2

All simulations use the released versions of the CCSM/CESM. CCSM4 incorporates Community Atmospheric and land Model version 4, Community Ice Code version 4, parallel ocean program version 2. CESM1 has an updated atmospheric component: Community Atmospheric model version 5. All the other model components remain the same as CCSM4. All model components of CESM2 have been updated. The model incorporates Community Atmospheric model version 6, Community Land Model version 5, Community Ice Code version 5, and updated parallel ocean program version 2 with major changes to the mixing schemes (Sun, Whitney, Bryan, & Tseng, 2017; Van Roekel et al., 2018). The model configurations of CCSM4 and CESM2 are consistent with the ones used for Climate Model Intercomparison Project (CMIP) 5 and 6.

Consistent with CMIP5 and 6 simulations, the atmosphere and land components are configured with the horizontal resolution of 0.9° latitude by 1.25° longitude. Atmosphere components of CCSM4, CESM1, and CESM2 respectively feature 26, 30, and 32 levels between ~992.6 hPa at the bottom and ~3.5 hPa at the top of the model. In all simulations, the ocean component features 60 vertical levels from 5 m depth to 5375 m depth. Both ocean and sea ice components use horizontal grid mesh of 384 by 320 grids with grid sizes identical to CMIP simulations north of ~60°S. Due to the “terrestrial presence” of western Antarctic ice sheet in PI and present-day boundary conditions, the 384 by 320 ocean and sea ice grid mesh does not cover the western Antarctic. In order to simulate ocean circulation and sea ice of the western Antarctic, we add 10 meridional rows of ocean grids to the present-day grid mesh. Each row is a replica of the southmost row of the 384 by 320 mesh. One may choose to generate new ocean grid mesh with the same number of grid cells but different grid sizes, which is commonly done in simulations of pre-Quaternary climates. However, different grid sizes may introduce artificial differences when comparing with the PI simulation, and hence, is not used here.

2.1.2 Boundary conditions

We implement enhanced boundary conditions following the protocol of PlioMIP2 (Haywood et al., 2015). We first calculate anomalies of MP topography and bathymetry relative to PI at 0.5° resolution (50 km). Both are derived from ETOPO dataset by PRISM4 project (Dowsett, Dolan, Rowley, Moucha, Forte, Mitrovica, Pound, Salzmann, Robinson, & Chandler, 2016a). Anomalies are then interpolated to the resolution of model components and added to the preindustrial topography and bathymetry used by CCSM/CESM. Due to the lack of information of high-resolution topographic roughness during the MP, modern roughness is mapped to paleotopography by proximity with the exception of where the ice sheets were absent during the MP. Topographic roughness from the nearest unglaciated land is prescribed to cover the deglaciated area of the Greenland and Antarctic.

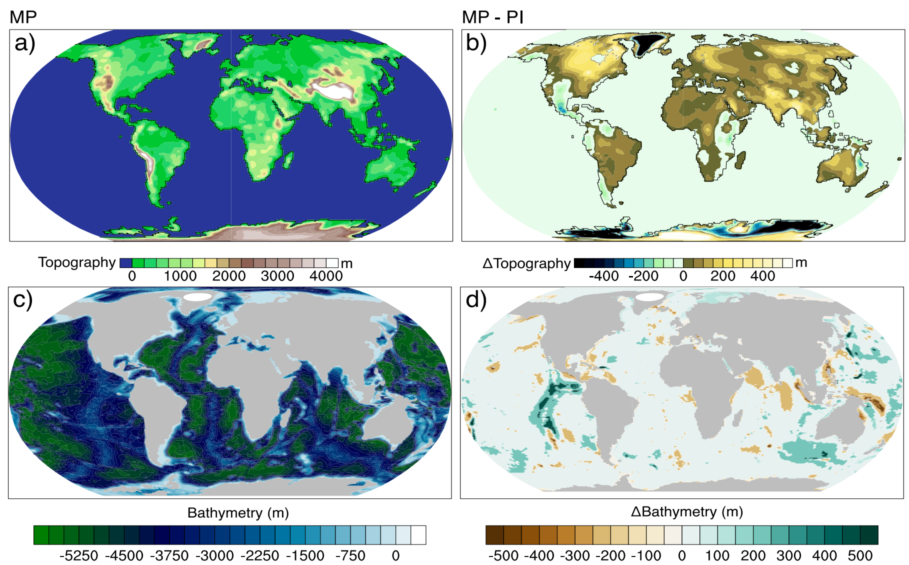

Figure 1 Model input of a) and c) MP topography and bathymetry and b) and d) differences from preindustrial following the PlioMIP2 protocol with enhanced boundary conditions.

MP changes to topography are typically less 500 meters (Fig. 1a and b). Bathymetric changes mainly occur in the newly open western Antarctic shelf, uplifted Mariana trench and East Pacific Rise, and alterations around marine time continents due to mantle convection. Coastlines are adjusted to feature closed Bering Strait and Arctic Archipelago straits, exposed Hudson Bay, Baltic sea shelf, Sunda and Sahul Shelf (Dowsett, Dolan, Rowley, Moucha, Forte, Mitrovica, Pound, Salzmann, Robinson, & Chandler, 2016a). Greenland and Antarctic ice sheet are largely reduced (Dolan et al., 2012) (Fig. 1c and d).

Although no change occurs in reconstructed biome types from PlioMIP1 to PlioMIP2 (Salzmann, Haywood, Lunt, Valdes, & Hill, 2008), we choose to use the more general mega-biome map for PlioMIP2 instead of the more detailed map used in CCSM4 PlioMIP1. We also update the mapping method to convert biome types to plant functional types (PFTs) used by CCSM/CESM. MP paleo-biome distribution is generated by blending the fossil records with BIOME4 simulations (Salzmann, Haywood, Lunt, Valdes, & Hill, 2008). Yet, CCSM4 and CESMs require PFTs as boundary conditions to solve productivity and plant phenology as part of the prognostic terrestrial carbon cycle in equilibrium with climate.

Our updated mapping method includes the following steps: 1) We group the modern PFTs ($PFT_{BIOME\text{-}present}$) into groups of modern megabiome types defined by BIOME4 (BIOME-present). 2) We quantify the latitudinal offset of the same megabiome type between its MP (BIOME-MP) and present-day location (BIOME-present) using the mean meridional Euclidian distance. 3) Interim maps of PFTs ($PFT_{BIOME\text{-}i}$) and megabiome types (BIOME-i) are generated by shifting $PFT_{BIOME\text{-}present}$ and BIOME-present to their MP latitudes. 4) We map the PFTs from the $PFT_{BIOME\text{-}i}$ to the final MP locations using spatial correspondence G: $PFT_{BIOME\text{-}MP} = G(PFT_{BIOME\text{-}i})$. G is determined with BIOME-MP = G(BIOME-i) by proximity and inverse distance weighting within a radius of 500 km. The second and third step are not included in the previous mapping

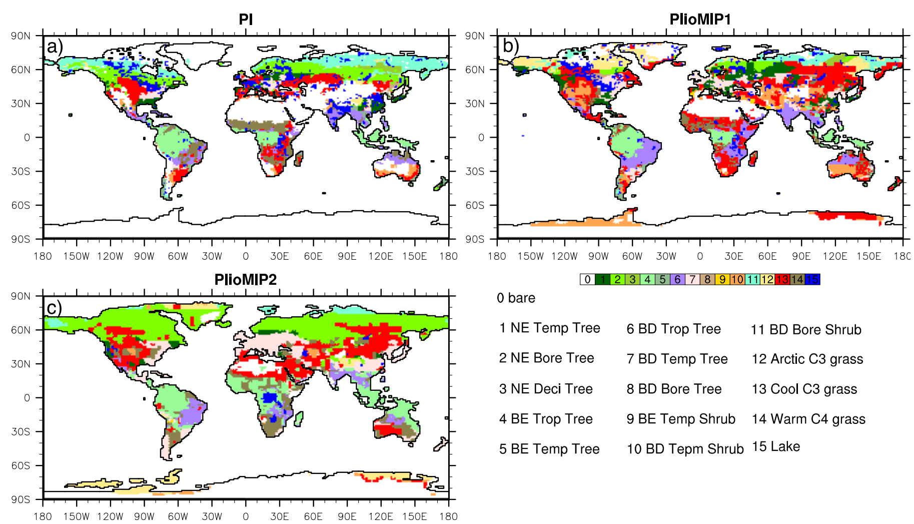

Figure 2 Dominant plant functional type (PFT) and lake mask (≥0.1 fraction) of model boundary conditions for a) preindustrial (PI) and MP simulations with b) the mapping method and biome map used in PlioMIP1 and c) the mapping method and biome map used in PlioMIP2. Dominant PFT is the PFT with the highest percentage among 15 possible PFTs within a grid cell.

method (Rosenbloom, Otto-Bliesner, Brady, & Lawrence, 2013b). Without these steps, MP PFTs corresponding to boreal forest biome are extrapolated from the northern edge of the present-day boreal forest by proximity, resulting in muted changes in PFTs (Fig. 2).

Using the same approach, we apply the MP soil map (Pound, Tindall, & Pickering, 2014a) to generate the soil color and soil organics in our MP simulation. MP lakes are prescribed according to reconstructions (Pound, Tindall, & Pickering, 2014a). Yet, in all CCSM4 and CESMs, lake water balance is maintained with the assumption of fixed lake depth (Oleson et al., 2010). Our test runs suggest that the atmospheric net water input cannot maintain the lake level of the Northern African lakes. Water from the nearest ocean, i.e., the Mediterranean, is extracted to maintain the lake level. To avoid this unphysical process, the Northern African lakes are not featured in our simulations (Fig. 2).

2.1.3 Implementation

All simulations are carried out on Cheyenne supercomputer (CISL, 2017a, b), which is maintained at Computational Information Systems Lab and funded by National Science Foundation. For CCSM4 and CESM1.2, we branch out two preindustrial (PI) simulations from the long simulations (1000 years) of PI performed on the now retired Yellowstone supercomputer using CCSM4 and CESM1.0. (Gent et al., 2011; Hurrell et al., 2013). These two PI simulations are continued for an additional 180 and 300 years on Cheyenne with the same model CCSM4 and slightly updated model CESM1.2. Changing supercomputer or small model updates create no change in the net top of the atmosphere (TOA) radiation imbalance (~0.1W/m^2) (Fig. 3a). Simulated global mean surface temperatures of PI are also consistent with published values (Fig. 3b). These two PI simulations (CCSM4-PI and CESM1.2-PI) serve the baseline for comparisons with MP simulations using respective models (CCSM4-MP and CESM1.2-MP). CESM2 PI simulation is recently completed on Cheyenne. This simulation serves as the baseline for comparisons with the CESM2-MP simulation (CESM2-MP).

Model initialization, forcing, run length, and terminal net TOA radiation imbalance are summarized in Table 1. Details of initialization of the land and ocean components are discussed here.

Table 1
Key Changes of Model Boundary Conditions, Forcing, and the End of Run Diagnostics in MP simulations

Boundary Conditions, Forcing, and the End of Run Diagnostics		Experiment information
Topography		PlioMIP2 enhanced
Model Versions		CCSM4, CESM1.2, CESM2
Resolution		~1°C for all components
Western Antarctic		Ocean with peninsular
Land Cover	Boundary Condition	MP mega-biome mapped to CLM PFTs
	Initiation	Land only spin-up
Ocean	Boundary Condition	PlioMIP2 enhanced with Closed Bering Strait, closed Canadian Arctic Archipelagoes, exposed Sunda and Salhu shelf
	Initiation	CCSM4: Preindustrial CESM1.2/CESM2: PRISM3D
Forcing Agents		CO_2: 400 ppm N_2O: 275.68 ppb CH_4:791.6 ppb Orbital forcing: 1990 AD Aerosol flux: 1850 AD
End of Run Diagnostics	Run Length	1200 years
	TOA Net Radiation Imbalance (Last 100 Years)	CCSM4: 0.04 W/m^2 CESM1.2: 0.13 W/m^2 CESM2: 0.21 W/m^2

To reduce the spin-up time of carbon cycle on land, we carried out separate land-only simulations with arbitrary initial conditions, and forcings generated by the coupled MP test runs using CESM1.2 (featuring Community Land Model version 4) and CESM2 (featuring Community Land Model version 5) respectively. Land initial conditions for these two test runs were interpolated from the PI runs. The rest of the boundary and forcing conditions are the same as the final runs. These two test runs were continued for ~200 years before producing the 30-year forcing data. This spin-up procedure is meant to reduce the runtime by producing a land initial state close to MP.

Due to the high computational expenses of CESM1.2 and CESM2, we test both preindustrial and warm initial conditions to determine a cost effective approach for ocean initialization. For the preindustrial initialization, 3D ocean temperature and salinity of equilibrium PI runs are mapped to the MP bathymetry based on proximity. For the warm initial conditions, we follow the method of previous PlioMIP1 simulation and use the PRISM paleo-SST reconstructions (Rosenbloom, Otto-Bliesner, Brady, & Lawrence, 2013a). Sea water temperature anomalies between MP paleo-SSTs and PI observations are added to the results of PI simulations to create the initial ocean temperature. Salinity is initialized from the published PlioMIP1 simulation (Rosenbloom, Otto-Bliesner, Brady, & Lawrence, 2013a).

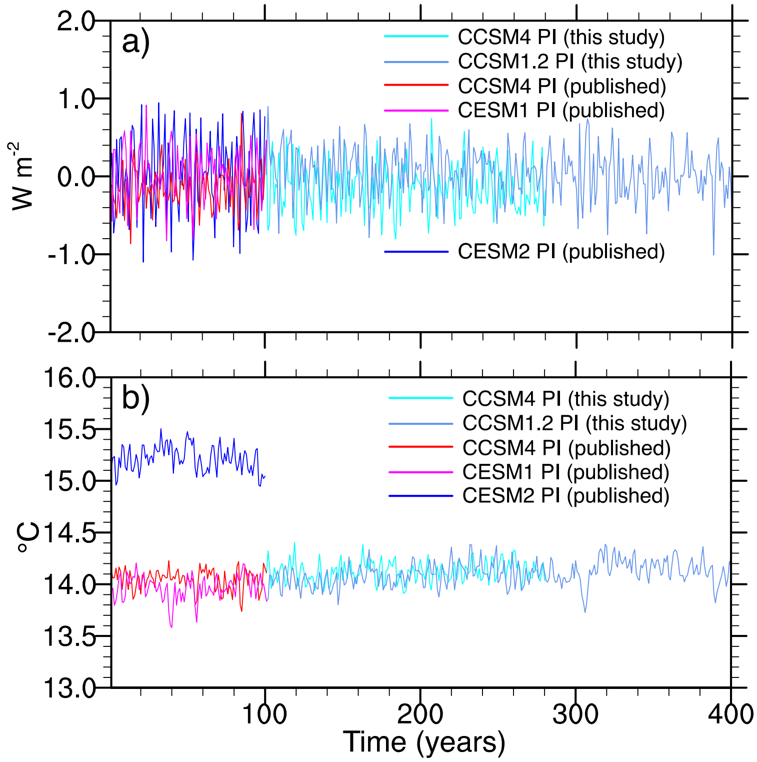

Figure 3 Time series of a) net top of the atmosphere (TOA) radiation imbalance and b) global mean surface temperature of preindustrial simulated by CCSM4, CESM1.2, and CESM2. Both CCSM4 and CESM1.2 preindustrial runs are branched from published cases done on an older supercomputer (Gent et al., 2011; Hurrell et al., 2013). CESM2 simulation has recently been completed on the same computer and published in this issue (only the last 100 year data is shown here).

For the PI initialization with CCSM4, TOA radiation imbalance declines rapidly within the first 50 years of simulations. TOA radiation imbalance remains high in both CESM1.2 and CESM2 even after over 100 simulation years. In comparison, warm initialization allows TOA radiation imbalance to start small in both CESM1.2 and CESM2 (Fig. 4). Thereby, these two simulations were carried out with warm initialization. Sea ice component is initialized with zero ice content in all simulations.

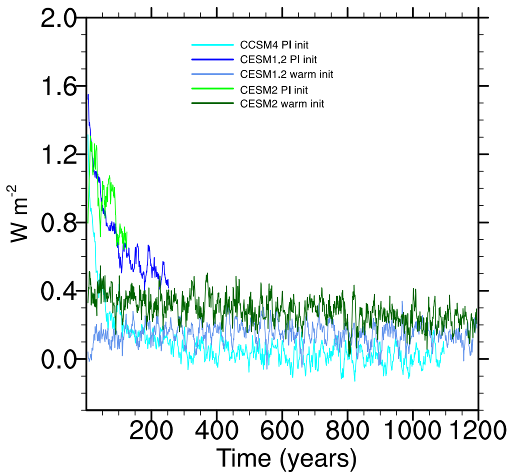

Figure 4 11-year running average of time series of the net top of the atmosphere radiation imbalance of MP simulations with ocean temperature initialized from warm (warm init) and PI (PI init) conditions.

2.1.4 Diagnostics of equilibrium

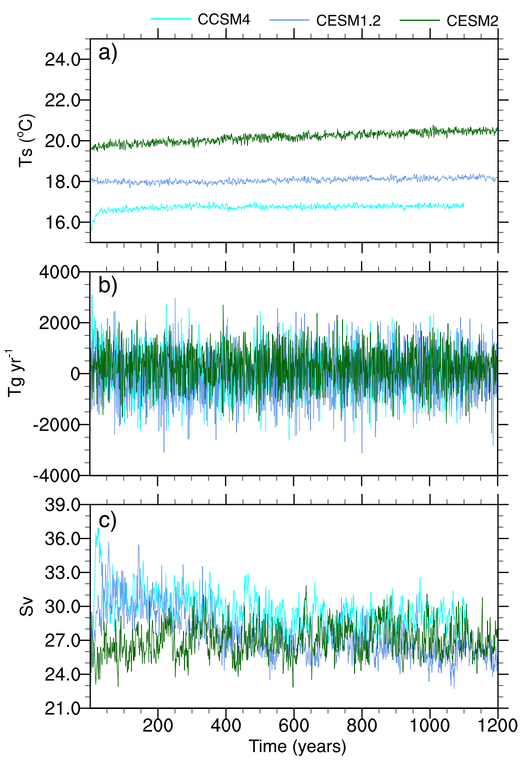

Figure 5 Time series of global mean surface temperature (Ts), net fluxes of ecosystem carbon exchange, and strength of the Atlantic Meridional Overturning Circulation (AMOC) in our MP simulations by CCSM4, CESM1.2, and CESM2.

MP simulations are run for over 1000 years. For the last 200 years of model simulations, TOA radiation imbalance has reached within ~0.1 W/m^2 of the published imbalance of the PI runs (~0.1 W/m^2) (Table 1), suggesting quasi-equilibrium. Model equilibrium is also assessed with trends of global mean surface temperature, net fluxes of ecosystem carbon exchange, and strength of the Atlantic Meridional Overturning Circulation (AMOC) for the final 200 simulation years (Fig. 5). The calculated trends are all within 5% change per century of the measured quantities. Nonetheless, global mean ocean temperatures have more detectable trends. This metric is known difficult to attain equilibrium even in multi-millennial simulations (Brady, Otto-Bliesner, Kay, & Rosenbloom, 2013; Rugenstein et al., 2019).

2.2 Analysis of results

MP climate change is quantified as the averaged differences of the last 100-year model simulations between the MP and PI runs using the same model. We calculate a series of climate metrics to quantify large-scale climate change. Model definitions or references of these metrics are provided in Table 2.

Table 2

Metrics Used in This Study to Quantify Large-scale Changes of MP Climate Relative to Preindustrial

Metrics	Model Definitions or References
Low Level Cloud	Cloud coverage below 700 hPa
Medium Level Cloud	Cloud coverage between 700 and 400 hPa
High Level Cloud	Cloud coverage above 400 hPa to 10 hPa
Total Hadley Circulation (HC) Strength ($I_{Had\text{-}tot}$)	Difference between the maximum and minimum of the zonal mean mass stream function between 30°N and 30°S (Oort & Yienger, 1996).
Northern Hemisphere HC strength ($I_{Had\text{-}N}$)	Maximum of the zonal mean mass stream function between 0° and 30°N (Oort & Yienger, 1996)
Southern Hemisphere HC Strength ($I_{Had\text{-}S}$)	Minimum of the zonal mean mass stream function between 30°S and 0° (Oort & Yienger, 1996)
Walker Circulation Strength (I_{Wal})	Difference between annual mean sea level pressure of 5°S to 5°N, 80°E to 180° and 5°S to 5°N, 80°W to 180° (Vecchi & Soden, 2007)
Equatorial west-east SST Contrast ($SST_{grad,\ W\text{-}S}$)	Differences between the annual mean sea surface temperature of 10°S – 10°N, 130°E – 170°E and 2°S – 2°N, 90°W – 140°W (Tierney et al., 2019)
Atlantic Meridional Overturning Circulation (AMOC) Strength	Northern hemispheric maximum of stream function achieved by integrating meridional velocity zonally across the Atlantic basin and vertically across the ocean depth coordinate e.g. (Frajka-Williams et al., 2019)
ΔAMOC Strength	Difference in steam function of the Atlantic basin is first calculated; maximum of the difference in the northern hemisphere below 500 m

3 Results

Metrics of simulated global mean surface conditions, moist state, and changes of the atmosphere and ocean circulation are shown in Table 3, 4, and 5. Model convergence and disagreements are described in the following.

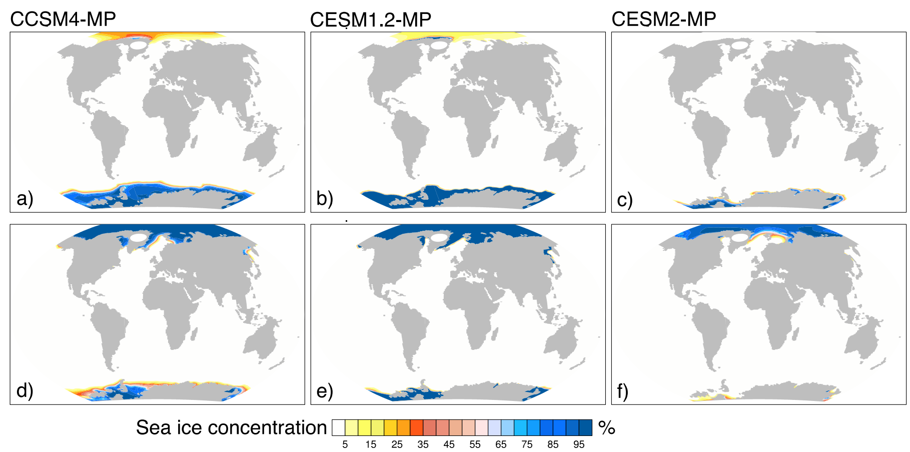

Figure 6 Mean sea ice concentration of a) to c) Arctic summer (August to October) and d) to f) Antarctic summer (February to April) simulated by MP simulations using three versions of the models.

3.1 Global mean surface climate

Among three versions of the simulations, CESM2-MP features the greatest change in the surface climate, CCSM4 features the least (Table 3). Global mean surface air temperature rises by 2.7 to 5.2°C relative to PI. In the tropics, surface warming is between 1.5 to 3.7°C, 55% to 70% of the global mean warming. SST increases by 1.7 to 3.9°C globally with 1.4 to 3.4°C increase in the tropics, ~82% to 87% of the global mean. Surface warming (both in the air temperature and SST)

Table 3

Changes of Global Mean Surface Climatology of MP Relative to PI simulated by CCSM4, CESM1.2 and CESM2.

	T_a (°C)	Ta_{Trop} (°C)	Ta_{Arctic} (°C)	$Ta_{Antarctic}$ (°C)	SST (90°N to 90°S) (°C)	SST (15°N to 15°S) (°C)	SST (40°N to 70°N) (°C)	SST (40°S to 70°S) (°C)	Annual Arctic Sea ice (10^6 km^2)	Annual Antarctic Sea ice (10^6 km^2)	August to October Arctic Sea ice (10^6 km^2)	February to April Antarctic Sea ice (10^6 km^2)
CCSM4-MP	2.7	1.5	8.1	6.5	1.7	1.4	4.4	2.3	-5.8 (-51.0%)	-5.0 (-31.6%)	0.6 (-91.8%)	5.6 (-45.1%)
CESM1.2-MP	4.0	2.6	12.3	9.8	2.9	2.4	5.7	3.7	-7.3 (-67.1%)	-7.2 (-61.3%)	0.01 (-99.9%)	1.9 (-63.4%)
CESM2-MP	5.2	3.7	12.6	12.0	3.9	3.4	7.3	4.6	-7.7 (-75.1%)	-8.2 (-81.0%)	0.002 (-100%)	0.4 (-91.1%)

Note. Numbers in parentheses highlight the % change relative to PI. T_a: global mean surface air temperature. Ta_{Trop}: 15°S – 15°N average of surface air temperature. Ta_{Arctic}: 70°N – 90°N average of surface air temperature. $Ta_{Antarctic}$: 70°S – 90°S average of the surface air temperature. SST: Sea surface temperature.

is strongly amplified towards the high latitudes with greater amplification in the northern high latitudes than the southern high latitudes. This warming pattern is consistent with previous findings of PlioMIP1 (Haywood, Hill, et al., 2013c) and paleo-observations (Dowsett et al., 2012). Moreover, our MP simulations feature substantial reduction in annual sea ice by 50.6% to 73.7% in the Arctic, and 31.6% to 81% in the Antarctic. In particular, Arctic Ocean is sea ice free during the boreal summer (August to October) in CESM1.2 and CESM2. Antarctic Ocean is nearly austral summer (February to April) sea ice free in CESM2 (Fig. 6) (Table 3).

Despite enhanced Arctic warming from CCSM4 to CESM2, the relative strength of the net feedback of the Arctic region to global mean decreases. Using the classic feedback framework (Goosse et al., 2018), the total feedback factor (γ), which measures the relative strength of all other feedbacks to the strength of Planck's feedback, can be estimated as: $\gamma = 1 - \frac{\Delta T_0}{\Delta T_s}$, ΔT_s is the surface temperature change; ΔT_0 is the surface temperature change due to Planck's feedback. γ scales positively with ΔT_s and negatively with ΔT_0. Due to the highly similar reference state of preindustrial, Planck's feedback is similar among our simulations, hence, intermodal differences in feedback factors scale with surface the temperature change relative to preindustrial: $\gamma \sim \Delta T_s$.

We use the ratio of Arctic (ΔT_{sp}) to global mean ΔT_s (ΔT_{sg}) to compare polar amplification of feedback strength between simulations. $\frac{\Delta T_{sp}}{\Delta T_{sg}}$ for the Arctic region is 3.0 in CCSM4 and CESM1.2 but only 2.4 in CESM2, suggesting weakened polar amplification of feedback strength. As a result, the enhanced surface warming in the Arctic region in CESM1.2 and CESM2 is not a result of polar amplification of feedback strength, but mainly a result of warmer global mean climate. Similar conclusion also applies to the Antarctic region. $\frac{\gamma_p}{\gamma_m}$ is consistent (within 0.1) among all MP simulations over this region despite enhanced Antarctic warming from CCSM4 to CESM2 (Table 3).

3.2 Precipitation and cloud

Global mean annual precipitation increases by 5.3% to 11.2% in MP simulations (Table 4). Relative precipitation increase to per degree of global mean surface warming is around 2%, consistent among models and with previous modeling studies (Held & Soden, 2006). This result suggests weakened convective mass overturning in response to surface warming (Held & Soden, 2006), which is also shown in the relative smaller increase in the convective precipitation by 3.1% to 7.5% compared to the increase of total precipitation.

Table 4
The Same as Table 3, but for Simulated Global Mean Moist State.

	% Change of mean troposphere specific humidity	Changes of mean troposphere temperature (°C)	% Change of mean tropospheric specific humidity per °C warming of the troposphere	Changes of Precipitation (cm/yr)	% Changes of Low cloud coverage	% Changes of middle cloud coverage	% Changes of high cloud coverage
CCSM4-MP	12.8	1.1	11.6	5.7 (+5.3%)	0.8	-0.2	0.5
CESM1.2-MP	19.1	2.2	8.7	9.5 (+8.5%)	-2.6	-2.2	-0.3
CESM2-MP	26.4	3.5	7.5	12.1 (+11.2%)	-4.7	-4.0	-0.5

Note. Numbers in parentheses highlight the % change relative to PI

Cloud coverage displays opposite changes between CCSM4-MP and two versions CESMs-MP. CCSM4-MP features small increase in low and high clouds. Yet, both CESM1.2-MP and CESM2-MP feature small reduction of clouds at all heights (Table 4). This inter-model disagreement may be explained by changes of tropospheric relative humidity. CCSM4-MP features 11.6% increase in specific humidity per degree warming, CESM1.2-MP and CESM2-MP features 8.7% and 7.5% increase per degree warming. The increase in specific humidity of CCSM4-MP far exceeds the increase in saturation vapor pressure (7% per degree warming), suggesting increase in relative humidity of the troposphere. This increase may compensate the effect of weakened convective mass overturning in CCSM4-MP, leading to a small increase in cloudiness. Yet, much smaller increase in relative humidity is shown in CESM1.2-MP and CESM2-MP, suggesting a lack of compensation.

3.3 Tropical Circulation change and model dependency

Consistent with weakened convective mass overturning, Hadley Circulation (HC) weakens in all MP simulations (Table 5) (Fig. 7). This weakening primarily occurs in the northern hemisphere by -10 to -20%. Southern hemisphere shows complex changes in HC morphology with much smaller changes in the overturning strength in all simulations (Table 5).

Table 5
The Same as Table 3, but for circulation changes.

	Changes of $I_{Had\text{-}tot}$ (10^9 kg m s^{-1})	Changes of $I_{Had\text{-}N}$ (10^9 kg m s^{-1})	Changes of $I_{Had\text{-}S}$ (10^9 kg m s^{-1})	% Change of I_{Wal}	$SST_{grad,\ W\text{-}S}$ (°C)	ΔAMOC Strength (Sv)
CCSM4-MP	-8.2 (-5.6%)	-7.8 (-10.1%)	+0.4 (-0.4%)	5.1	0.2	7.6
CESM1.2-MP	-12.1 (-6.7%)	-9.3 (-11.7%)	+2.9 (-2.8%)	-0.7	-0.3	3.4
CESM2-MP	-19.1 (-10.1%)	-16.9 (-21.6%)	+2.2 (-2.0%)	-9.0	-1.0	6.9

Note. Metrics used to quantify circulation changes are shown in Table 2. Numbers in parentheses highlight the % change relative to PI.

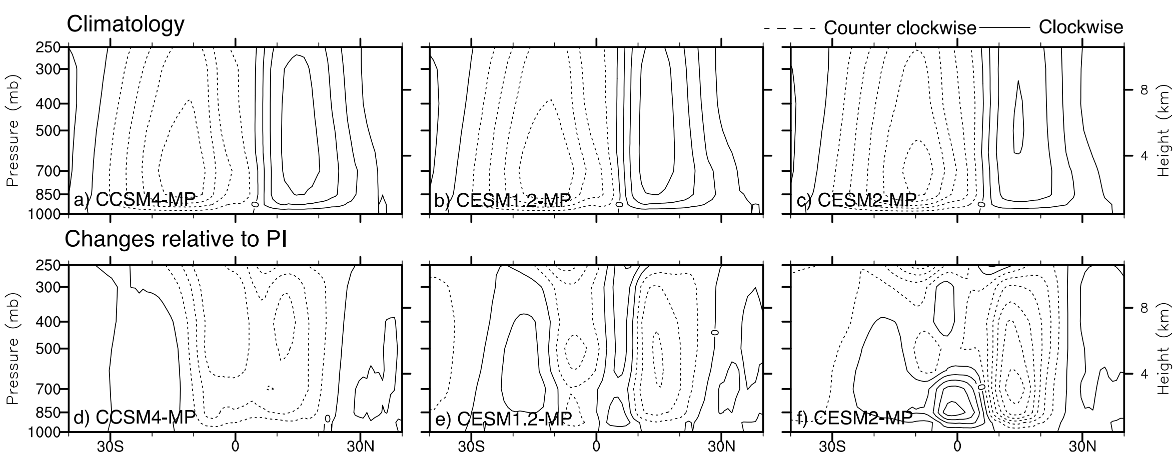

Figure 7 Simulated a) to c) MP annual climatology and d) to f) changes of zonal mean mass stream function in the tropics by three different versions of CCSM/CESM models. Changes are relative to preindustrial simulations with the same model. Contours in a) to c) are at $2\text{x}10^{10}$ kg/s and in d) to f) are at $3\text{x}10^{9}$kg/s.

This hemispherically asymmetric weakening of HC seemingly coincides with hemispherically asymmetric change in meridional SST structure. In the northern hemisphere, mean SST contrast between the tropics (15°S – 15°N) and extratropics (40°N – 70°N) decreases by ~3 - 4°C in all three simulations (Table 1). This contrast only decreases by ~1°C in the southern hemisphere. The correspondence between changes in the meridional SST structure and the strength or symmetry of the HC has been proposed based on previous experiments with prescribed SSTs

(Brierley et al., 2009; Carrapa, Clementz, & Feng, 2019; Feng, Poulsen, & Werner, 2016), and radiation flux adjustments (Burls & Fedorov, 2017; Frierson & Hwang, 2012; Frierson et al., 2013). This connection can be established through meridional heat transport: heating from the extratropical ocean can alter the radiation imbalance of the atmosphere between the hemispheres (Frierson et al., 2013) or between the tropics and extratropics (Burls & Fedorov, 2017; Carrapa et al., 2019), leading to changes in the hemispheric symmetry (Frierson et al., 2013) or strength of the atmospheric heat transport and HC (Burls & Fedorov, 2017; Carrapa et al., 2019).

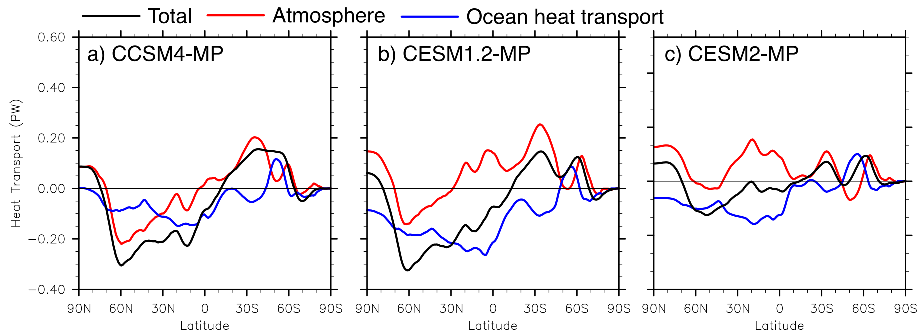

Figure 8 Simulated annual changes of total, atmosphere, and ocean meridional heat transport between MP and preindustrial simulations by three versions of models.

The proposed linkage between meridional heat transport and HC strength does not explain the intermodal differences in simulated northern hemisphere HC strength. From CCSM4-MP to CESM2-MP, despite a greater weakening of the northern hemisphere HC strength, changes in the northern hemisphere extratropical atmospheric heat transport goes from strong reduction (CCSM4) to nearly constant (CESM2) compared to PI (Fig. 8).

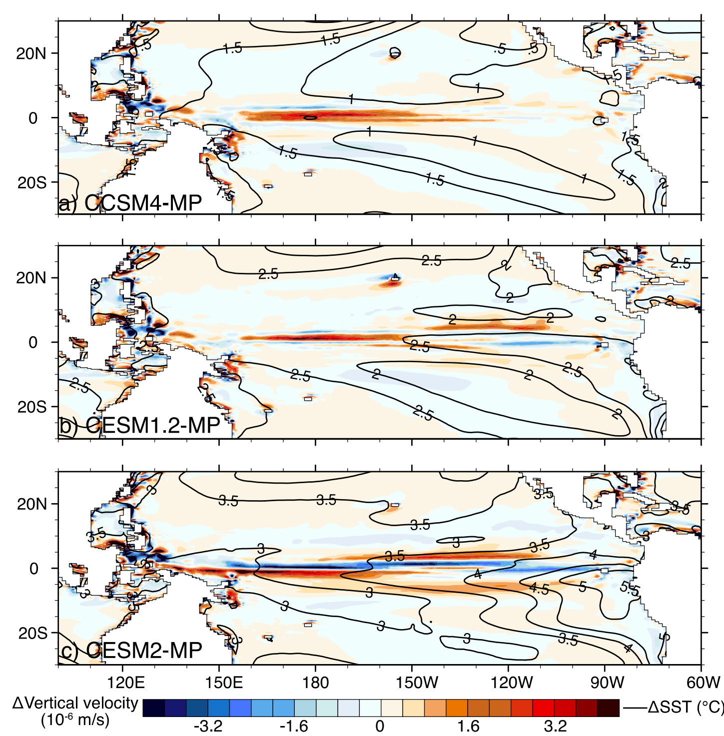

Figure 9 Simulated annual changes of SST and vertical velocity of sea water averaged from 5 cm to 110 m relative to the preindustrial.

Model dependency is seen clearly in simulated MP Walker circulation changes. CCSM4-MP simulates strengthened Walker circulation, whereas, CESM1.2-MP and CESM2-MP simulate small (-0.2%) to substantial (-9.0%) weakening of the Walker circulation (Table 3). This inter-model spread is well coupled to the inter-model spread of changes in the east-west SST contrast across the equatorial Pacific. This SST contrast increases by 0.3°C in CCSM4-MP, but decreases by 0.3°C and 1°C in CESM1.2-MP and CESM2-MP (Fig. 9). In the later versions of models, MP upwelling in the upper ocean of the eastern equatorial Pacific also weakens (Fig. 9). Consequently, coupled equatorial atmosphere-ocean state becomes more El Niño-like in both CESM1.2-MP and CESM2-MP, but remains unchanged in CCSM4. Paleo-observations support a more El Niño-like state (Fedorov et al., 2013; Tierney et al., 2019)

3.4 Atlantic Meridional Overturning Circulation (AMOC)

All MP simulations show strengthened AMOC compared to PI. Strengthened AMOC corresponds to increased salinity in the north Atlantic (Fig. 10). This result is consistent with previous sensitivity studies with closure of the Arctic ocean gateways of Bering Strait and Canadian Arctic Archipelago straits (Otto-Bliesner et al., 2017). Closure of Arctic ocean gateways

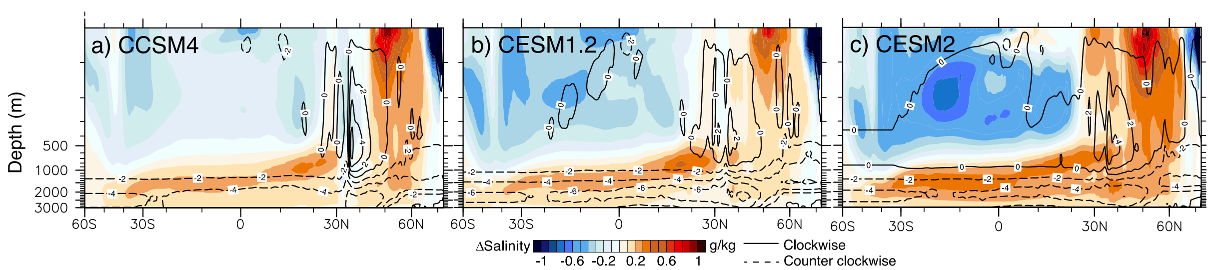

Figure 10 Simulated changes of zonal mean mass stream function of the Atlantic ocean basin relative to pre-industrial (contour), and 82°W to 38°E averaged changes of salinity (shaded) relative to pre-industrial.

restricts the fresher water export from the Arctic towards the north Atlantic, and hence, weakens the overall vertical stratification of the North Atlantic. The consistent responses between previous studies, which only quantify the effect of closure of the gateways, and ours, which incorporates the full spectrum of changes of MP boundary conditions, highlight the importance of Arctic Ocean gateways in modulating the strength of AMOC. The effect of CO_2 and other boundary condition changes on simulated MP AMOC strength is likely secondary.

4 Discussion

4.1 Enhanced Earth System Sensitivity from CCSM4 to CESM2

Earth System Sensitivity (ESS) describes the long-term equilibrium surface temperature response to a doubling of CO_2, which measures long-term feedbacks from changes in ocean circulation, vegetation distribution, and ice sheet in addition to short-term feedbacks, but excludes feedbacks from carbon cycle such as marine productivity or weathering (Lunt et al., 2009). ESS estimated from MP simulations is known to be greater than the equilibrium climate sensitivity (ECS) (Haywood, Hill, et al., 2013c; Lunt et al., 2009). ECS mainly measures sub-millennial scale feedbacks in the climate system.

Disregarding millennial time scale feedbacks from the ocean, vegetation, and ice sheet, one may approximate the amount of global mean warming due to CO_2 increase using ECS. Radiative forcing from the MP CO_2 (400 ppm) relative to preindustrial (284.7 ppm) is ~1.82W/m_2. ECSs are 3.2°C (Bitz et al., 2012), 4.0°C (Gettelman et al., 2012), and 5.3°C (Gettelman et al., 2019) per doubling of CO_2 for CCSM4, CESM1.2, and CESM2. Using the MP CO_2 forcing and ECSs of individual models, we expect global mean warming of 1.6°C, 2.0°C, and 2.6°C in CCSM4-MP, CESM1.2-MP, and CESM2-MP. These estimates are much smaller than the warming simulated by these experiments (Table 2).

We argue that the amplified warming among MP experiments reflects enhanced ESS going from CCSM4 to CESM2. In our simulations, vegetation and ice sheet are prescribed based on geological reconstructions of "true" equilibrium earth system, and hence, are part of the ESS. Changes in topography, soil, and lakes reflect plate tectonics and weathering, and are irrelevant to ESS. However, topographic changes are generally small, ranging from a minimum of -280 m to a maximum of 528.6 m in all simulations. Global mean surface temperature responses to MP changes in soil and lake distribution (Pound, Tindall, & Pickering, 2014a), and Arctic ocean gateways (Feng et al., 2017; Otto-Bliesner et al., 2017) are also shown small. Hence, global mean model responses largely reflect enhanced ESS. This enhancement is up to 70% of ECS-estimated warming in CCSM4, and up to 100% in both CESM1.2 and CESM2 (Table 2).

This result highlights the long-term warming potential of the Earth System at millennial time scale. From CCSM4 to CESM2, there is a clear amplification of ESS beyond the increase of ECS. Geological reconstructions of warm periods of Neogene (since 23 millions of years ago) may support a high ESS. For example, global mean SST is estimated to be 5 – 6°C warmer than preindustrial during the early-to-middle Miocene (Goldner, Herold, & Huber, 2014), yet CO_2 estimates are mostly under 500 ppm (Foster, Lear, & Rae, 2012; Londoño et al., 2018).

4.2 Can paleo-observations of MP SSTs help evaluate skills of CCSM4-MP, CESM1.2-MP, and CESM2-MP?

An important goal of Paleoclimate modeling is to sample model structural uncertainties with a set of boundary and forcing conditions outside the model calibration range (e.g., (Haywood, Valdes, Aze, Barlow, Burke, Dolan, Heydt, Hill, Jamieson, & Otto-Bliesner, 2019b)). Comparisons between model simulations and paleo-observations can provide insights into model skills (Haywood, Valdes, Aze, Barlow, Burke, Dolan, Heydt, Hill, Jamieson, & Otto-Bliesner, 2019b; Kageyama et al., 2018). In practice, this exercise is often complicated by the uncertainty and sparsity of paleo-observations.

With coordinated effort, a new MP SST compilation is now available through compiling data within a narrow age constraint of 3 thousand years of the targeted MP interval (Foley and Dowsett, 2019). This dataset eliminates the uncertainty due to unresolved glacial-interglacial cycles in the records, which are shown to cause major ambiguity when comparing with model simulations (Feng et al., 2017; Prescott et al., 2014; Salzmann et al., 2013). Here, we use this dataset to help rank skills of different MP simulations by CCSM/CESMs.

4.2.1 Assessment of global mean surface air temperature

Among all simulations, global mean surface air temperature anomalies ($\Delta\{Ta\}_{global\text{-}model}$) scales linearly with the simulated anomalies of SSTs averaged across paleo-observation sites ($\Delta\{SST\}_{sites\text{-}model}$) (Fig. 11). Both $\Delta\{Ta\}_{global\text{-}model}$ and $\Delta\{SST\}_{sites\text{-}model}$ are calculated by subtracting the last 100-year averages of PI simulations (constant for each experiment) from the MP averages taken for each 30-yr period of the last 600-year model data, resulting in 20 pairs of $\Delta\{Ta\}_{global\text{-}model}$ and $\Delta\{SST\}_{sites\text{-}model}$ for each experiment. Treating each pair of $\Delta\{Ta\}_{global\text{-}model}$ and $\Delta\{SST\}_{sites\text{-}model}$ as one realization of climate mean state, we construct regressions of

$\Delta\{Ta\}_{global\text{-}model}$ as a function of $\Delta\{SST\}_{sites\text{-}model}$ for all simulations. The result shows an excellent linear fit (Fig. 11).

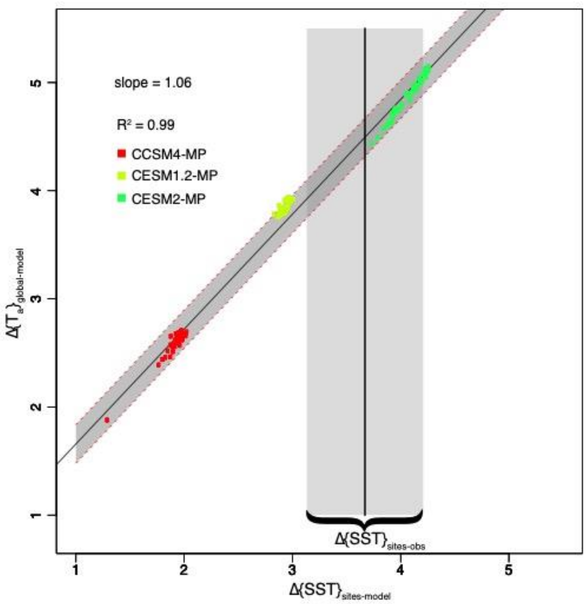

Figure 11 Regression of model simulated global mean surface air temperature anomaly ($\Delta\{T_a\}_{global\text{-}model}$) with respect to simulated SST anomalies averaged over the paleo-observational sites ($\Delta\{SST\}_{sites\text{-}model}$) for each 30-yr period of the last 600 model years. Anomalies are calculated with respect to pre-industrial simulations. Shadings show 95% likelihood prediction interval. The mean and one standard deviation of the SST anomaly estimated with the actual paleo-observation data and 1871-1900 mean of HadISST are also shown ($\Delta\{SST\}_{sites\text{-}obs}$).

We further calculate observed mean SST anomalies across the paleo-observation sites ($\Delta\{SST\}_{sites\text{-}obs}$) by subtracting instrumental observations of SSTs averaged over 1871 to 1900 using the HadISST data (Rayner et al., 2003) from observed SSTs at paleo-observation sites. The one standard deviation (1σ) of paleo-observations are propagated to the 1σ the $\Delta\{SST\}_{site\text{-}obs}$ assuming Gaussian distributions of paleo-observations and site independency. $\Delta\{SST\}_{sites\text{-}obs}$ is estimated to be 3.6±0.6 °C.

Based on the estimated values of $\Delta\{SST\}_{sites\text{-}obs}$ and the linear relationship between $\Delta\{Ta\}_{global\text{-}model}$ and $\Delta\{SST\}_{sites\text{-}model}$, we find that global mean warming is underestimated by CCSM4-MP, but close to CESM1.2 (slight underestimate) and CESM2 (slight overestimate) (Fig. 11). This result supports the higher ESS estimated by CESM1.2 and CESM2 than CCSM4. Yet, the ESS is potentially underestimated by CESM1.2 and overestimated by CESM2.

4.2.2 Assessment of meridional SST structure

A key spatial signature of the MP SST warming is the northern high latitude amplification. SST changes are muted in the tropics and is relatively small in the southern high latitudes compared to the northern high latitudes (Dowsett et al., 2012; Haywood, Hill, et al., 2013c). This meridional structure is known challenging for CCSM4 to capture (Feng et al., 2017; Rosenbloom, Otto-Bliesner, Brady, & Lawrence, 2013a) (Fig. 12).

In order to quantify the meridional warming structure, we apply polynomial fit using sin(φ) as the basis (φ: latitude in radian) to quantify latitudinal distribution of paleo-SST anomalies relative to the 1871 – 1990 averages (ΔSST_{obs}) (Fig. 12). The choice of sin(φ) is to account for the hemispherically asymmetric amplification of the SST warming. Statistically significant fit is achieved with the second order polynomial. P-value is 0.03 through the likelihood ratio test against an intercept-only model. The polynomial fit captures the strongly amplified warming in the northern high latitudes recorded in paleo-observations.

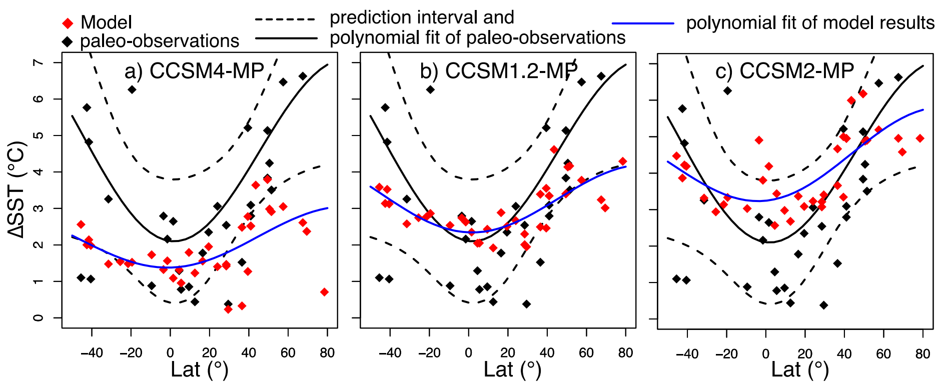

Figure 12 Second order polynomial fit of the SST anomalies at paleo-observation sites as a function of sine latitude. Anomalies are departures from the preindustrial SSTs. Black: second order polynomial fit to paleo-observations and 95% likelihood prediction interval. Blue: second order polynomial fit to model simulations.

The second-order polynomial fit is also applied to simulated latitudinal distribution of SST anomalies relative to PI gathered from the paleo-SST sites (ΔSST_{model}). The fit to the ΔSST_{model} shows latitudinally more uniform warming than the fit to ΔSST_{model}. Among simulations, CESM1.2-MP and CESM2-MP (Fig. 12b and c) show more enhanced SST warming in the northern high latitudes than the CCSM4-MP, providing a closer match to the spatial structure of ΔSST_{obs} (Fig. 12a).

Nonetheless, there is large zonal heterogeneity of ΔSST_{obs}. Accounting for this zonal heterogeneity gives a wide 95% confidence interval of the polynomial fit, which encloses 32 out of 37 ΔSST_{model} of CESM1.2 and 34 out of 37 ΔSST_{model} of CESM2 (Fig. 12b and c). Consequently, we cannot rule out the possibility that SST warming structures in CESM1.2 MP and CESM2 MP are statistically similar to paleo-observations. In contrast, nearly half of the

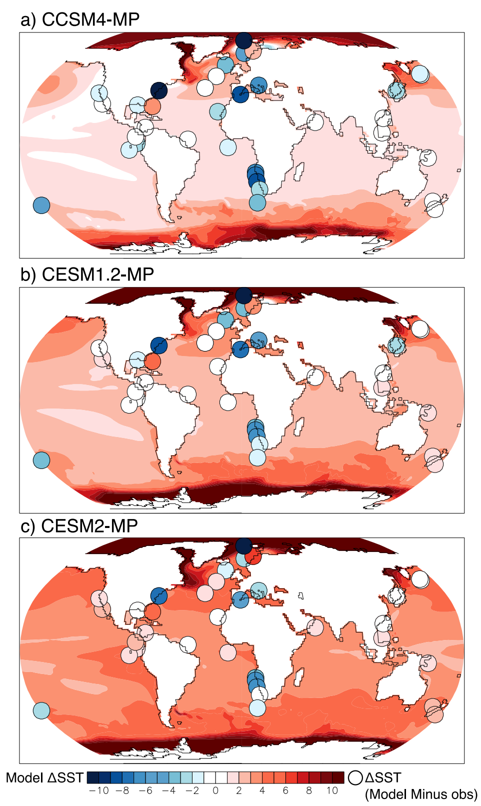

Figure 13 Differences between MP and preindustrial SSTs (**Δ**SST) in our simulations (shaded) and differences in **Δ**SST between simulations and paleo-observations (filled circles). **Δ**SST is calculated separately from model data and observations before taking the difference to estimate **Δ**SST (Model minus obs). Filled circles share the same color bar as the shaded areas.

ΔSST_{model} from CCSM4 MP is outside the confidence interval of paleo-observations, suggesting a lack of fit (Fig. 12a).

Fig. 13 shows the spatial distribution of ΔSST_{model} and ΔSST_{obs}. From CCSM4-MP to CESM2-MP, ΔSST_{model} displays a closer match to ΔSST_{obs} in the tropics and northern high latitudes. Major model-observation mismatch occurs around Benguela current, Gulf Stream, and North Atlantic current, which may be attributable to the high spatial heterogeneity of ocean conditions following the currents and insufficient model resolution. High-resolution simulations by CCSM4 and CESM1 have shown to improve skills at simulating present-day upwelling and current systems (Gent, Yeager, Neale, Levis, & Bailey, 2009; Small et al., 2014).

5 Conclusions

Three versions of Earth System Models maintained at National Center for Atmospheric Research are applied to simulate mid-Piacenzian warm period, a target interval of Paleoclimate Model Intercomparison Project. All three simulations agree in the signs of MP changes of global mean and meridional structure of surface temperature, precipitation, sea ice cover, Hadley Circulation, and Atlantic meridional overturning circulation relative to preindustrial. Among simulations, CCSM4 features the smallest changes and CESM2 features the greatest. Specifically, global mean surface air temperature increases by 2.7°C in CCSM4 and 5.2°C in CESM2. Surface warming is amplified in the polar region with Arctic amplification of 3 times global mean in CCSM4 and CESM1.2, and 2.4 times in CESM2. CESM2 also features near complete sea ice free conditions during both Arctic and Antarctic summer. Summer sea ice remains present in both Arctic and Antarctic in CCSM4. Precipitation increases from 5% in CCSM4 to 11% in CESM2 relative to PI, slower than the expected increase from saturation vapor pressure, suggesting slowing down of convective mass overturning in all MP simulations. Hadley circulation weakens by 10 to 22% in the northern hemisphere. AMOC strengthens by 3 to 8 Sv. All simulations demonstrate greater Earth System sensitivity (ESS) compared to the Equilibrium Climate Sensitivity (ECS). ESS is amplified by 70% in CCSM4 and 100% in CESM1.2 and CESM2 relative to ECS.

Simulations disagree in the signs of global mean cloud changes: CCSM4 shows small increase in both low and high cloud covers; both CESM1.2 and CESM2 show reduction of cloud covers at all heights. Disagreement also occurs in the Walker circulation and changes of mean climate state of the equatorial Pacific. CCSM4-MP shows strengthened Walker circulation, and unchanged mean climate state of the equatorial Pacific relative to preindustrial. Both CESM1.2-MP and CESM2-MP show weakened Walker circulation and changes towards a more El Niño-like equatorial Pacific state.

Finally, we explore the possibility of using paleo-observations of MP SSTs to evaluate the performances of our MP simulations. MP global mean surface warming is largely underestimated by CCSM4, but close to CESM1.2 and CESM2, supporting the enhanced ESS by these models. Yet, the warming is slightly underestimated by CESM1.2, but overestimated by CESM2. Both CESM1.2 and CESM2 are also better at capturing the northern high latitude amplification of the SST warming than CCSM4. Nonetheless, all three models have difficulty at capturing observed SSTs near the Benguela current, Gulf Stream, and North Atlantic current, which may be attributable to the insufficient model resolution.

Acknowledgments and Data

The authors are grateful for the helpful insights about paleo-observation data from Harry Dowsett, PlioMIP2 boundary condition design from Alan Haywood and Aisling Dolan, estuary box model from Y.-H. Tseng, land model boundary conditions from Erik Kluzek, land model initialization from Keith Olson, and land model debugging from Bill Sacks. We would also like to acknowledge high-performance computing support from Cheyenne (doi:10.5065/D6RX99HX) provided by NCAR's Computational and Information Systems Laboratory, sponsored by the National Science Foundation. This research is sponsored by NSF grant 1903650 to R. Feng, 1418411 to Bette L.

Otto-Bliesner. Simulation data are available to download through Campaign storage of Cheyenne supercomputer using the Globus endpoint: /glade/campaign/cesm/development/palwg/pliocene. CESM2 run is available through Earth System Grid, and is part of NCAR's contribution to CMIP6. The CESM project is supported primarily by the National Science Foundation (NSF). This material is based upon work supported by the National Center for Atmospheric Research (NCAR), which is a major facility sponsored by the NSF under Cooperative Agreement No. 1852977. Computing and data storage resources, including the Cheyenne supercomputer (doi:10.5065/D6RX99HX), were provided by the Computational and Information Systems Laboratory (CISL) at NCAR.

References

Danabasoglu, G., Lamarque, J. -F., Bachmeister, J., Bailey, D. A., DuVivier, A. K., Edwards, J., Emmons, L. K., Fasullo, J., Garcia, R., Gettelman, A., Hannay, C., Holland, M. M., Large, W. G., Lawrence, D. M., Lenaerts, J. T. M., Lindsay, K., Lipscomb, W. H., Mills, M. J., Neale, R., Oleson, K. W., Otto-Bliesner, B., Phillips, A. S., Sacks, W., Tilmes, S., van Kampenhout, L., Vertenstein, M., Bertini, A., Dennis, J., Deser, C., Fischer, C., Fox-Kember, B., Kay, J. E., Kinnison, D., Kushner, P. J., Long, M. C., Mickelson, S., Moore, J. K., Nienhouse, E., Polvani, L., Rasch, P. J., Strand, W. G. The Community Earth System Model version 2 (CESM2). *Manuscript submitted for publication to Journal of Advances in Modeling Earth Systems*

Foley, K.M., and Dowsett, H.J., 2019, Community sourced mid-Piacenzian sea surface temperature (SST) data: U.S. Geological Survey data release, https://doi.org/10.5066/P9YP3DTV

Bitz, C. M., Shell, K. M., Gent, P. R., Bailey, D. A., Danabasoglu, G., Armour, K. C., et al. (2012). Climate sensitivity of the community climate system model, version 4. *Journal of Climate*, *25*(9), 3053–3070.

Bogenschutz, P. A., Gettelman, A., Morrison, H., Larson, V. E., Craig, C., & Schanen, D. P. (2013). Higher-order turbulence closure and its impact on climate simulations in the Community Atmosphere Model. *Journal of Climate*, *26*(23), 9655–9676.

Brady, E. C., Otto-Bliesner, B. L., Kay, J. E., & Rosenbloom, N. (2013). Sensitivity to glacial forcing in the CCSM4. *Journal of Climate*, *26*(6), 1901–1925.

Brierley, C. M., Fedorov, A. V., Liu, Z., Herbert, T. D., Lawrence, K. T., & LaRiviere, J. P. (2009). Greatly Expanded Tropical Warm Pool and Weakened Hadley Circulation in the Early Pliocene. *Science*, *323*(5922), 1714–1718. http://doi.org/10.1126/science.1167625

Burls, N. J., & Fedorov, A. V. (2017). Wetter subtropics in a warmer world: Contrasting past and future hydrological cycles. *Proceedings of the National Academy of Sciences*, *114*(49), 12888–12893.

Carrapa, B., Clementz, M., & Feng, R. (2019). Ecological and hydroclimate responses to strengthening of the Hadley circulation in South America during the Late Miocene cooling. *Proceedings of the National Academy of Sciences*, *116*(20), 9747–9752.

Computational and Information Systems Laboratory. 2017a. Cheyenne: HPE/SGI ICE XA System (Climate Simulation Laboratory). Boulder, CO: National Center for Atmospheric Research. doi:10.5065/D6RX99HX.

Computational and Information Systems Laboratory. 2017b. Cheyenne: HPE/SGI ICE XA System (University Community Computing). Boulder, CO: National Center for Atmospheric Research. doi:10.5065/D6RX99HX.

Coats, S., & Karnauskas, K. B. (2017). Are simulated and observed twentieth century tropical Pacific sea surface temperature trends significant relative to internal variability? *Geophysical Research Letters*, *44*(19), 9928–9937.

Collins, M., Knutti, R., Arblaster, J., Dufresne, J.-L., Fichefet, T., Friedlingstein, P., et al. (2013). Long-term climate change: projections, commitments and irreversibility, 1029–1136.

Dolan, A. M., Koenig, S. J., Hill, D. J., Haywood, A. M., & DeConto, R. M. (2012). Pliocene ice sheet modelling intercomparison project (PLISMIP)–experimental design. *Geoscientific Model Development*, *5*(4), 963–974.

Dowsett, H. J., Robinson, M. M., Haywood, A. M., Hill, D. J., Dolan, A. M., Stoll, D. K., et al. (2012). Assessing confidence in Pliocene sea surface temperatures to evaluate predictive models. *Nature Climate Change*, *2*(5), 365–371. http://doi.org/10.1038/NCLIMATE1455

Dowsett, H. J., Robinson, M. M., Stoll, D. K., Foley, K. M., Johnson, A. L. A., Williams, M., & Riesselman, C. R. (2013). The PRISM (Pliocene palaeoclimate) reconstruction: time for a paradigm shift. *Philosophical Transactions of the Royal Society of London a: Mathematical, Physical and Engineering Sciences*, *371*(2001), 20120524. http://doi.org/10.1098/rsta.2012.0524

Dowsett, H., Dolan, A., Rowley, D., Moucha, R., Forte, A. M., Mitrovica, J. X., Pound, M., Salzmann, U., Robinson, M., & Chandler, M. (2016a). The PRISM4 (mid-Piacenzian) paleoenvironmental reconstruction. *Climate of the Past*, *12*(7), 1519–1538.

Dowsett, H., Dolan, A., Rowley, D., Moucha, R., Forte, A. M., Mitrovica, J. X., Pound, M., Salzmann, U., Robinson, M., & Chandler, M. (2016b). The PRISM4 (mid-Piacenzian) paleoenvironmental reconstruction. *Climate of the Past*, *12*(7), 1519–1538.

Dowsett, H., Robinson, M., Haywood, A. M., Salzmann, U., Hill, D., Sohl, L. E., et al. (2010). The PRISM3D paleoenvironmental reconstruction. *Stratigraphy*, *7*(2-3), 123–139.

Fedorov, A. V., Brierley, C. M., Lawrence, K. T., Liu, Z., Dekens, P. S., & Ravelo, A. C. (2013). Patterns and mechanisms of early Pliocene warmth. *Nature*, *496*(7443), 43–49. http://doi.org/10.1038/nature12003

Feng, R., Otto-Bliesner, B. L., Fletcher, T. L., Tabor, C. R., Ballantyne, A. P., & Brady, E. C. (2017). Amplified Late Pliocene terrestrial warmth in northern high latitudes from greater radiative forcing and closed Arctic Ocean gateways. *Earth and Planetary Science Letters*, *466*, 129–138.

Feng, R., Otto-Bliesner, B. L., Xu, Y., Brady, E., Fletcher, T., & Ballantyne, A. (2019). Contributions of aerosol-cloud interactions to mid-Piacenzian seasonally sea ice-free Arctic Ocean. *Geophysical Research Letters*.

Feng, R., Poulsen, C. J., & Werner, M. (2016). Tropical circulation intensification and tectonic extension recorded by Neogene terrestrial δ18O records of the western United States. *Geology*, *44*(11), 971–974.

Fisher, R. A., Wieder, W. R., Sanderson, B. M., Koven, C. D., Oleson, K. W., Xu, C., et al. (2019). Parametric controls on vegetation responses to biogeochemical forcing in the CLM5. *Journal of Advances in Modeling Earth Systems*, *11*(9), 2879–2895.

Foster, G. L., Lear, C. H., & Rae, J. W. (2012). The evolution of pCO2, ice volume and climate during the middle Miocene. *Earth and Planetary Science Letters*, *341*, 243–254.

Frajka-Williams, E., Ansorge, I. J., Baehr, J., Bryden, H. L., Chidichimo, M. P., Cunningham, S. A., et al. (2019). Atlantic Meridional Overturning Circulation: Observed transports and variability. *Frontiers in Marine Science*, *6*, 260.

Frierson, D. M., & Hwang, Y.-T. (2012). Extratropical influence on ITCZ shifts in slab ocean simulations of global warming. *Journal of Climate*, *25*(2), 720–733.

Frierson, D. M., Hwang, Y.-T., Fučkar, N. S., Seager, R., Kang, S. M., Donohoe, A., et al. (2013). Contribution of ocean overturning circulation to tropical rainfall peak in the Northern Hemisphere. *Nature Geoscience*, *6*(11), 940.

Gent, P. R., Danabasoglu, G., Donner, L. J., Holland, M. M., Hunke, E. C., Jayne, S. R., et al. (2011). The community climate system model version 4. *Journal of Climate*, *24*(19), 4973–4991. http://doi.org/10.1175/2011JCLI4083.1

Gent, P. R., Yeager, S. G., Neale, R. B., Levis, S., & Bailey, D. A. (2009). Improvements in a half degree atmosphere/land version of the CCSM. *Climate Dynamics*, *34*(6), 819–833. http://doi.org/10.1007/s00382-009-0614-8

Gettelman, A., Hannay, C., Bacmeister, J. T., Neale, R. B., Pendergrass, A. G., Danabasoglu, G., et al. (2019). High Climate Sensitivity in the Community Earth System Model Version 2 (CESM2). *Geophysical Research Letters*, *46*(14), 8329–8337.

Gettelman, A., Kay, J. E., & Fasullo, J. T. (2013). Spatial Decomposition of Climate Feedbacks in the Community Earth System Model. *Journal of Climate*, *26*(11), 3544–3561. http://doi.org/10.1175/JCLI-D-12-00497.1

Gettelman, A., Kay, J. E., & Shell, K. M. (2012). The evolution of climate sensitivity and climate feedbacks in the Community Atmosphere Model. *Journal of Climate*, *25*(5), 1453–1469.

Goldner, A., Herold, N., & Huber, M. (2014). The challenge of simulating the warmth of the mid-Miocene climatic optimum in CESM1. *Climate of the Past*, *10*, 536. http://doi.org/10.5194/cp-10-523-2014

Goosse, H., Kay, J. E., Armour, K. C., Bodas-Salcedo, A., Chepfer, H., Docquier, D., et al. (2018). Quantifying climate feedbacks in polar regions. *Nature Communications*, *9*(1), 1919.

Haywood, A. M., Dolan, A. M., Pickering, S. J., Dowsett, H. J., McClymont, E. L., Prescott, C. L., Salzmann, U., Hill, D. J., Hunter, S. J., & Lunt, D. J. (2013a). On the identification of a Pliocene time slice for data–model comparison. *Philosophical Transactions of the Royal Society of London a: Mathematical, Physical and Engineering Sciences*, *371*(2001), 20120515.

Haywood, A. M., Dolan, A. M., Pickering, S. J., Dowsett, H. J., McClymont, E. L., Prescott, C. L., Salzmann, U., Hill, D. J., Hunter, S. J., Lunt, D. J., et al. (2013b). On the identification of a Pliocene time slice for data-model comparison. *Philosophical Transactions of the Royal Society of London a: Mathematical, Physical and Engineering Sciences*, *371*(2001), –20120515. http://doi.org/10.1098/rsta.2012.0515

Haywood, A. M., Dowsett, H. J., & Dolan, A. M. (2015). Pliocene Model Intercomparison (PlioMIP) Phase 2: scientific objectives and experimental design. *Climate of the Past*.

Haywood, A. M., Hill, D. J., Dolan, A. M., Otto-Bliesner, B. L., Bragg, F., Chan, W. L., et al. (2013c). Large-scale features of Pliocene climate: results from the Pliocene Model Intercomparison Project. *EPIC3Clim. Past, Copernicus Publications, 9, Pp. 191-209, ISSN: 1814-9324*. http://doi.org/10.5194/cp-9-191-2013

Haywood, A. M., Valdes, P. J., Aze, T., Barlow, N., Burke, A., Dolan, A. M., Heydt, Von Der, A. S., Hill, D. J., Jamieson, S., & Otto-Bliesner, B. L. (2019a). What can Palaeoclimate Modelling do for you? *Earth Systems and Environment*, *3*(1), 1–18.

Haywood, A. M., Valdes, P. J., Aze, T., Barlow, N., Burke, A., Dolan, A. M., Heydt, Von Der, A. S., Hill, D. J., Jamieson, S., & Otto-Bliesner, B. L. (2019b). What can Palaeoclimate Modelling do for you? *Earth Systems and Environment*, *3*(1), 1–18.

Haywood, A., Dowsett, H., Otto-Bliesner, B., Chandler, M., Dolan, A., Hill, D., et al. (2010). Pliocene model intercomparison project (PlioMIP): experimental design and boundary conditions (experiment 1). *Geoscientific Model Development*, *3*(1), 227–242.

Held, I. M., & Soden, B. J. (2006). Robust responses of the hydrological cycle to global warming. *Journal of Climate*.

Hurrell, J. W., Holland, M. M., Gent, P. R., Ghan, S., Kay, J. E., Kushner, P. J., et al. (2013). The community earth system model: a framework for collaborative research. *Bulletin of the American Meteorological Society*, *94*(9), 1339–1360.

Kageyama, M., Braconnot, P., Harrison, S. P., Haywood, A. M., Jungclaus, J., Otto-Bliesner, B. L., et al. (2018). PMIP4-CMIP6: the contribution of the Paleoclimate Modelling Intercomparison Project to CMIP6. *Geoscientific Model Development Discussions*, *11*(3), 1033–1057.

Kay, J. E., Hillman, B. R., Klein, S. A., Zhang, Y., Medeiros, B., Pincus, R., et al. (2012). Exposing global cloud biases in the Community Atmosphere Model (CAM) using satellite observations and their corresponding instrument simulators. *Journal of Climate*, *25*(15), 5190–5207.

Liu, X., Easter, R. C., Ghan, S. J., Zaveri, R., Rasch, P., Shi, X., et al. (2012). Toward a minimal representation of aerosols in climate models: Description and evaluation in the Community Atmosphere Model CAM5. *Geoscientific Model Development*, *5*(3), 709.

Londoño, L., Royer, D. L., Jaramillo, C., Escobar, J., Foster, D. A., Cárdenas Rozo, A. L., & Wood, A. (2018). Early Miocene CO 2 estimates from a Neotropical fossil leaf assemblage exceed 400 ppm. *American Journal of Botany*, *105*(11), 1929–1937.

Lunt, D. J., Haywood, A. M., Schmidt, G. A., Salzmann, U., Valdes, P. J., & Dowsett, H. J. (2009). Earth system sensitivity inferred from Pliocene modelling and data. *Nature Geoscience*, *3*(1), 60–64. http://doi.org/10.1038/ngeo706

Masson-Delmotte, V., Schulz, M., Abe-Ouchi, A., Beer, J., Ganopolski, A., González Rouco, J. F., et al. (2013). Information from paleoclimate archives. *Climate Change*, *383464*, 2013.

Oleson, K. W., Lawrence, D. M., Gordon, B., Flanner, M. G., Kluzek, E., Peter, J., et al. (2010). Technical description of version 4.0 of the Community Land Model (CLM).

Oort, A. H., & Yienger, J. J. (1996). Observed interannual variability in the Hadley circulation and its connection to ENSO. *Journal of Climate*, *9*(11), 2751–2767.

Otto-Bliesner, B. L., Jahn, A., Feng, R., Brady, E. C., Hu, A., & Löfverström, M. (2017). Amplified North Atlantic warming in the late Pliocene by changes in Arctic gateways. *Geophysical Research Letters*, *44*(2), 957–964.

Pithan, F., & Mauritsen, T. (2014). Arctic amplification dominated by temperature feedbacks in contemporary climate models. *Nature Geoscience*, *7*(3), 181.

Pound, M. J., Tindall, J., & Pickering, S. J. (2014a). Late Pliocene lakes and soils: a global data set for the analysis of climate feedbacks in a warmer world. *Climate of the …*.

Pound, M. J., Tindall, J., Pickering, S. J., Haywood, A. M., Dowsett, H. J., & Salzmann, U. (2014b). Late Pliocene lakes and soils: a global data set for the analysis of climate feedbacks in a warmer world. *Climate of the Past*, *10*(1), 167–180.

Prescott, C. L., Haywood, A. M., Dolan, A. M., & Hunter, S. J. (2014). Assessing orbitally-forced interglacial climate variability during the mid-Pliocene Warm Period. *Earth and Planetary ….*

Rayner, N., Parker, D. E., Horton, E. B., Folland, C. K., Alexander, L. V., Rowell, D. P., et al. (2003). Global analyses of sea surface temperature, sea ice, and night marine air temperature since the late nineteenth century. *Journal of Geophysical Research*, *108*(D14).

Rosenbloom, N. A., Otto-Bliesner, B. L., Brady, E. C., & Lawrence, P. J. (2013a). Simulating the mid-Pliocene Warm Period with the CCSM4 model. *Geoscientific Model Development*, *6*(2), 549–561. http://doi.org/10.5194/gmd-6-549-2013

Rosenbloom, N. A., Otto-Bliesner, B. L., Brady, E. C., & Lawrence, P. J. (2013b). Simulating the mid-Pliocene Warm Period with the CCSM4 model. *Geoscientific Model Development*, *6*(2), 549–561. http://doi.org/10.5194/gmd-6-549-2013

Rugenstein, M., Bloch Johnson, J., Gregory, J., Andrews, T., Mauritsen, T., Li, C., et al. (2019). Equilibrium climate sensitivity estimated by equilibrating climate models. *Geophysical Research Letters*.

Salzmann, U., Dolan, A. M., Haywood, A. M., Chan, W.-L., Voss, J., Hill, D. J., et al. (2013). Challenges in quantifying Pliocene terrestrial warming revealed by data–model discord. *Nature Climate Change*, *3*(11), 969.

Salzmann, U., Haywood, A. M., Lunt, D. J., Valdes, P. J., & Hill, D. J. (2008). A new global biome reconstruction and data-model comparison for the Middle Pliocene. *Global Ecology and Biogeography*, *17*(3), 432–447. http://doi.org/10.1111/j.1466-8238.2008.00381.x

Seager, R., Cane, M., Henderson, N., Lee, D.-E., Abernathey, R., & Zhang, H. (2019). Strengthening tropical Pacific zonal sea surface temperature gradient consistent with rising greenhouse gases. *Nature Climate Change*, *9*(7), 517.

Small, R. J., Bacmeister, J., Bailey, D., Baker, A., Bishop, S., Bryan, F., et al. (2014). A new synoptic scale resolving global climate simulation using the Community Earth System Model. *Journal of Advances in Modeling Earth Systems*, *6*(4), 1065–1094.

Stroeve, J. C., Kattsov, V., Barrett, A., Serreze, M., Pavlova, T., Holland, M., & Meier, W. N. (2012). Trends in Arctic sea ice extent from CMIP5, CMIP3 and observations. *Geophysical Research Letters*, *39*(16).

Sun, Q., Whitney, M. M., Bryan, F. O., & Tseng, Y.-H. (2017). A box model for representing estuarine physical processes in Earth system models. *Ocean Modelling*, *112*, 139–153.

Tierney, J. E., Haywood, A. M., Feng, R., Bhattacharya, T., & Otto-Bliesner, B. L. (2019). Pliocene warmth consistent with greenhouse gas forcing. *Geophysical Research Letters*.

Turner, A. K., & Hunke, E. C. (2015). Impacts of a mushy-layer thermodynamic approach in global sea-ice simulations using the CICE sea-ice model. *Journal of Geophysical Research: Oceans*, *120*(2), 1253–1275.

Van Roekel, L., Adcroft, A. J., Danabasoglu, G., Griffies, S. M., Kauffman, B., Large, W., et al. (2018). The KPP Boundary Layer Scheme for the Ocean: Revisiting Its Formulation and Benchmarking One-Dimensional Simulations Relative to LES. *Journal of Advances in Modeling Earth Systems*, *10*(11), 2647–2685.

Vecchi, G. A., & Soden, B. J. (2007). Global warming and the weakening of the tropical circulation. *Journal of Climate*, *20*(17), 4316–4340. http://doi.org/10.1175/JCLI4258.1